

# Local gravitational redshifts can bias cosmological measurements

Radosław Wojtak,<sup>a,b</sup> Tamara M. Davis,<sup>c</sup> and Jophiel Wiis<sup>b</sup>

<sup>a</sup>Kavli Institute for Particle Astrophysics and Cosmology, Stanford University, SLAC National Accelerator Laboratory, Menlo Park, CA 94025

<sup>b</sup>Dark Cosmology Centre, Niels Bohr Institute, University of Copenhagen, Denmark

<sup>c</sup>School of Mathematics and Physics, University of Queensland, QLD 4072, Australia

E-mail: [wojtak@stanford.edu](mailto:wojtak@stanford.edu)

**Abstract.** Measurements of cosmological parameters via the distance-redshift relation usually rely on models that assume a homogenous universe. It is commonly presumed that the large-scale structure evident in our Universe has a negligible impact on the measurement if distances probed in observations are sufficiently large (compared to the scale of inhomogeneities) and are averaged over different directions on the sky. This presumption does not hold when considering the effect of the gravitational redshift caused by our local gravitational potential, which alters light coming from all distances and directions in the same way. Despite its small magnitude, this local gravitational redshift gives rise to noticeable effects in cosmological inference using SN Ia data. Assuming conservative prior knowledge of the local potential given by sampling a range of gravitational potentials at locations of Milky-Way-like galaxies identified in cosmological simulations, we show that ignoring the gravitational redshift effect in a standard data analysis leads to an additional systematic error of  $\sim 1\%$  in the determination of density parameters and the dark energy equation of state. We conclude that our local gravitational field affects our cosmological inference at a level that is important in future observations aiming to achieve percent-level accuracy.

---

## Contents

<b>1</b>	<b>Introduction</b>	<b>1</b>
<b>2</b>	<b>Gravitational Redshift</b>	<b>2</b>
2.1	Gravitational redshift from cosmological simulations	4
2.2	Time dependence of the gravitational redshift	6
2.3	Observers in extreme environments	7
<b>3</b>	<b>Effect of gravitational redshift in analysis of SN Ia data</b>	<b>8</b>
3.1	Predictions for systematic errors	11
<b>4</b>	<b>Discussion and conclusions</b>	<b>13</b>

---

## 1 Introduction

When standing on the surface of the Earth, one’s observations are strongly influenced by one’s location. Even such fundamental things as the strength of gravity, differ depending on whether you are on a mountain-top, in a valley, or sitting over an ore deposit. To get an unbiased measurement, one needs to make measurements in many different places – or take into account the local environment during the analysis.

In cosmology, too, our local environment influences our view of the universe as a whole. The universe is arguably more homogeneous than the surface of the Earth, which is why the cosmological principle (that the universe is homogeneous and isotropic) has been a very successful basis of our studies of the expansion of the universe. However, in this era of ‘precision cosmology’ the inhomogeneities are no longer as negligible as they once were. We are now at the stage where, to get accurate measurements of cosmological parameters, we need to take these inhomogeneities into account [e.g. 1–5].

Gravitational lensing and peculiar velocities are the primary observational manifestations of structure in the universe (apart from observing that structure itself). For cosmological purposes, many of the effects will average out over many observations in many directions. For example peculiar velocities of distant galaxies will not strongly effect the cosmological measurements from supernovae, despite the fact that they are shifting the observed redshift from the true cosmological redshift, because this essentially adds random scatter, which averages out. Similarly, lensing of supernova light will strongly magnify a few supernovae and slightly de-magnify most supernovae, because there is more volume in voids than clusters, but even though the scatter about the Hubble diagram is not gaussian, the mean remains unbiased [6, 7].

The one effect that does not cancel, however, is the effect of our own location in this landscape of space. Observations of our local universe suggest that we live in a slight underdensity, compared to the mean density of the universe. The first observational indication of a local underdensity was shown in the data of supernovae Ia [8, 9]. This reasoning, however, happened to depend strongly on modeling the supernovae colors [10]. Many prevalent arguments

for a local underdensity come from studies of galaxy counts [11–16] and galaxy cluster counts [17] in the local universe. If true, this would add a slight gravitational redshift to every redshift we measure, even those well outside our local density fluctuation. It also means that peculiar velocities of local galaxies will tend to be away from us (being sucked out of our underdensity), thus increasing the apparent Hubble flow of our local universe. The former of those effects – the gravitational redshift of our own underdensity – is the more important of the two for distant cosmological probes, because it affects every redshift we see from distant galaxies systematically. Although the gravitational redshift we expect is very small ( $\sim 10^{-5}$ ), it can still have a noticeable effect on our cosmological parameter measurements because it is systematic.

Gravitational redshift on cosmological scales was first detected in galaxy clusters [18–21]. The redshift manifests itself as relative shifts of the galaxy velocity distributions at different distances from the cluster center [for more details see 22–25]. The measured gravitational redshift is consistent with typical depths of the gravitational potential well in cluster-mass dark matter haloes, i.e. approximately  $4 \times 10^{-5}$  for haloes with virial masses of  $10^{14} M_{\odot}$ . Comparable values of the gravitational redshift are expected from large-scale structures. The gravitational redshift on these scales is expected to give rise to asymmetric features in the cross-correlation function of massive galaxies with lower mass galaxies, which should be detectable in upcoming redshifts surveys [26].

The purpose of this paper is to estimate the magnitude of the gravitational redshift effect, and estimate the impact it has on our cosmological inferences. We begin in Section 2 by estimating the typical magnitude of gravitational redshift that light experiences as it travels from emitters to us, and assessing what part of that does not cancel out on average. We consider light emitted from the mean gravitational potential of the universe, as well as light emitted from the mean gravitational potential of emitters, which are biased tracers of the potential (typically emitters sit in stronger gravitational wells because that is where galaxies form).

In Section 3 we assess the impact such a systematic shift in redshift would have on our cosmological inferences from supernova surveys. We show how the impact changes as more flexibility is added to the models (e.g. allowing a varying equation of state). Although the effect of a local gravitational redshift is small, it remains potentially important if we want to measure cosmological parameters to 1% precision, and could cause false tensions between data sets. We discuss these issues and conclude in Section 4.

## 2 Gravitational Redshift

The gravitational redshift results from a difference in a gravitational potential between the point of light reception and emission. In the weak field limit, the gravitational redshift  $z_g$  is given by

$$z_g = \frac{\phi_r - \phi_e}{c^2}, \quad (2.1)$$

where  $\phi_r$  and  $\phi_e$  is the gravitational potential at the points of light reception and emission, respectively. The gravitational redshift may take a positive or negative sign, depending on whether photons escape from a potential well or they are received therein. In the latter case, the gravitational redshift would be observed as a blueshift. We hereafter refer to both

situations as the gravitational redshift and we differentiate both by sign: positive for redshift and negative for blueshift.

In cosmological context, the gravitational redshift is directly related to inhomogeneities in the matter distribution. The redshift can be calculated using equation (2.1) with the peculiar gravitational potential given by the Poisson equation

$$\nabla^2\phi = 4\pi G a^2 \bar{\rho} \delta(x, t), \quad (2.2)$$

where  $a$  is the scale factor normalised to one at the present day,  $\bar{\rho}$  is the mean background density (mass per physical volume, so  $\bar{\rho} = \bar{\rho}_0 a^{-3}$ ), the density contrast is  $\delta = \rho/\bar{\rho} - 1$ , and the gradient is with respect to comoving coordinates [27].

Before we proceed with more detailed calculations, it is instructive to make a few simple estimates of the gravitational redshift for typical large-scale structures such as superclusters or cosmic voids. Approximating the matter distribution with a top-hat model, one can show that the peculiar gravitational potential is given by

$$\phi = \frac{G\Delta M}{R} = -\delta_R \Omega_m H_0^2 R^2/2, \quad (2.3)$$

where  $\Delta M$  is the total mass excess (decrement) with respect to the background density contribution,  $R$  is the radius of a structure,  $\delta_R$  is the total overdensity (the mean density contrast within  $R$ ),  $\Omega_m$  is the matter density parameter. We consider parameters characterizing two examples of observed large-scale structures:  $\delta_R = 0.8$  and  $R = 50 h^{-1}$  Mpc for the most massive superclusters similar to the Shapley Supercluster [28],  $\delta_R = -0.3$  and  $R = 100 h^{-1}$  Mpc corresponding to large cosmic voids. This yields  $\phi/c^2 = -3 \times 10^{-5}$  and  $\phi/c^2 = 5 \times 10^{-5}$  for the supercluster and the void, respectively. These are quite typical values of the gravitational redshift due to large-scale structures. Depending on the position of observer in the cosmic web, the gravitational redshift may be as large as  $10^{-4}$  (or 30 km/s, when expressed in terms of the approximate Doppler velocity  $z_g c$ ). It is interesting to notice that this value is comparable to the observed gravitational redshift due to deep potential wells in the most massive dark matter haloes associated with galaxy clusters [18, 20, 21]. This means that our simple estimate of the gravitational redshift can be boosted by factor of 2 when considering light emitted from massive galaxy clusters embedded in large superclusters.

Contrary to the density field, the amplitude of the peculiar gravitational potential does not decay with increasing scale. This can be shown by considering the variance of matter density fluctuations – and thus potential fluctuations – at large smoothing scales. In this regime, the power spectrum can be approximated by  $P(k) \propto k^n$ , where  $n$  is the spectral index of the primordial matter density fluctuations. For a top-hat window, the rms of the mass fluctuations within spheres of radius  $R \propto M^{1/3}$  is given by  $\sigma_M(R) \propto R^{-(3+n)/2}$  [29]. Conversion into the rms of the potential fluctuations yields the following scaling relation:  $\sigma_\phi(R) = G\sigma_M(R)M/R \propto R^{(1-n)/2}$ . For the Harrison-Zeldovich power spectrum ( $n = 1$ ), the rms of the potential fluctuations remains the same at all scales (in the limit of large scales) with  $\sigma_\phi/c^2 \approx 2 \times 10^{-5}$  for  $\Omega_m = 0.3$  and the power spectrum normalised to  $\sigma_8 = 0.8$  (approximately the measured rms of matter density fluctuations at a scale of  $8h^{-1}$  Mpc).

For a spectral index  $n < 1$ , the fluctuations start to grow at large scales. This persistent lack of vanishing of large-scale Fourier modes is a dramatically different property compared to the density field. Arguably the most striking consequence of it is the fact that in terms

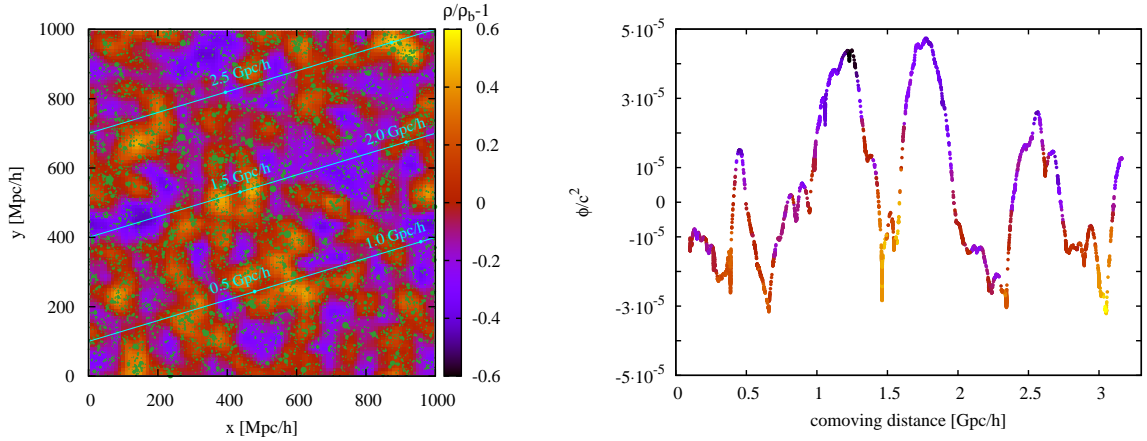


**Figure 1.** A density contrast map from a MultiDark simulation smoothed at a scale of  $50h^{-1}\text{Mpc}$  (left panel); with the peculiar gravitational potential of dark matter particles along a beam-sized line crossing the simulation box (right panel). The color coding on both panels indicates consistently the smoothed density contrast. The green filled circles on the left panel show the positions of dark matter haloes along the sight-line chosen. Their sizes are proportional to the virial radii. Fluctuations of the gravitational potential reflects large-scale inhomogeneities of the matter distribution, whereas sharp minima coincide with massive dark matter haloes. Humps and troughs in the potential encompass regions dominated by gravitational collapse (superclusters) and evacuation of matter (voids), respectively.

of the peculiar potential, the Universe is inhomogeneous at all scales. From a practical point of view, this property also shows that all calculations involving large-scale gravitational potential should include primarily large-scale Fourier modes. In particular, this implies the necessity of using cosmological simulations run in reasonably large boxes, with a side length of at least  $\sim 1h^{-1}\text{Gpc}$ .

## 2.1 Gravitational redshift from cosmological simulations

Exact theoretical calculations of the gravitational redshift should take into account non-linear evolution of cosmic structures. The reason is twofold. First, one should expect non-negligible contribution to the potential from structures evolving in strictly non-linear regime, e.g. clusters in superclusters. Second, realistic predictions for observations should be based on a mock catalog of galaxies which define in a natural way a set of observed objects as well as locations of observers in the cosmic web.

For our calculation of the gravitational redshift, we employ a large-scale cosmological  $N$ -body simulation from the MultiDark data base.<sup>1</sup> The simulation follows the evolution of  $2048^3$  dark matter particles in a volume of  $(1h^{-1}\text{Gpc})^3$ . The particle mass is  $8.7 \times 10^8 h^{-1}M_\odot$ , yielding a minimum resolved halo mass of around  $10^{11}h^{-1}M_\odot$ . The simulation adopted cosmological parameters determined from the fifth data release of WMAP satellite observations [31], i.e.  $\Omega_m = 0.27$ ,  $\Omega_\Lambda = 0.73$ ,  $\sigma_8 = 0.82$ .

<sup>1</sup>The simulation is publicly available through the MultiDark database (<http://www.multidark.org>). See [30] for all details of the database.

As the first step of the calculation, we compute the peculiar gravitational potential at positions of all particles. The potential is computed with the Poisson solver built in the Gadget code [32]. The right panel of Fig. 1 shows the gravitational potential of DM particles along a beam-size sight line crossing the simulation box at redshift  $z = 0$  (see the left panel). The color coding indicates the density contrast smoothed at a scale of  $50h^{-1}\text{Mpc}$ . It is clearly readable that the potential profile is determined primarily by two effects: fluctuations due to large-scale structures at scales of  $\geq 100h^{-1}\text{Mpc}$  and local minima coinciding with the positions of massive dark matter haloes. As expected, minima of the potential occur at places undergoing the process of collapse (positive density contrast), whereas the maxima coincide with regions dominated by the process of matter evacuation (negative density contrast). The amplitude of the large-scale fluctuations is consistent with our simple estimates of the potential obtained for voids and superclusters with the matter distribution approximated by a top-hat function.

The gravitational redshift is a differential effect for which one needs to specify positions where light is emitted and received. It is natural to think that both places should be located in galaxies. In order to generate a catalog of galaxies we apply an HOD (Halo Occupation Distribution) model to the catalog of dark matter haloes found in the simulation. We use all distinct haloes (haloes which are not subhaloes of larger haloes) detected by the Bound-Density-Maxima halo finder [33]. We assume that every halo has one central galaxy and a number of satellite galaxies. The satellite number for a given halo mass is drawn from a Poisson distribution whose mean is a power-law function of the halo mass. Parameters defining the mass dependance of the mean number of the satellites are taken from [34]. Once the galaxy catalog is generated, every galaxy is assigned the mean gravitational potential of all dark matter particles within the virial sphere of its host dark matter halo.

The gravitational redshift depends on the position of observer and selection of observed galaxies. The most straightforward way to quantify this effect is to consider a set of observers and a set of observed galaxies, and then to compute the distribution of mean (averaged over the same set of galaxies) gravitational redshifts as measured by these observers. In this approach, the gravitational redshift corresponds a difference between the gravitational potential at the observer's position and the mean potential at locations of all observed galaxies. Its distribution reflects directly the distribution of observers in the cosmic web (subject to a fixed observational selection). The same approach was recently used to study cosmic variance of the local determination of the Hubble constant [35].

We begin with a general setup for the calculation: observers located in Milky-Way-like galaxies and observing all galaxies found in the simulation at redshift  $z = 0$  what corresponds to a complete and shallow (no redshift evolution) galaxy survey. The Milky-Way galaxies are identified as the central galaxies of dark matter haloes with masses  $(1 - 2.5) \times 10^{12}h^{-1}\text{M}_{\odot}$ , where the adopted mass range comes from recent observational constraints on the Milky-Way halo mass [36]. The black line in Fig. 2 shows the resulting distribution of the gravitational redshift (the same set of galaxies observed by observers located at different positions in the simulation box). The distribution is determined by the positions of observers in the cosmic web. Depending on whether observers are located in overdense or underdense regions, light from the observed galaxies becomes respectively blueshifted (negative values) or redshifted (positive values). The most likely value of the gravitational redshift is close to 0, while 95 per cent of the allowed gravitational redshifts range between  $\pm 4 \times 10^{-5}$  ( $z_{\text{gc}} = \pm 12 \text{ km/s}$ ).

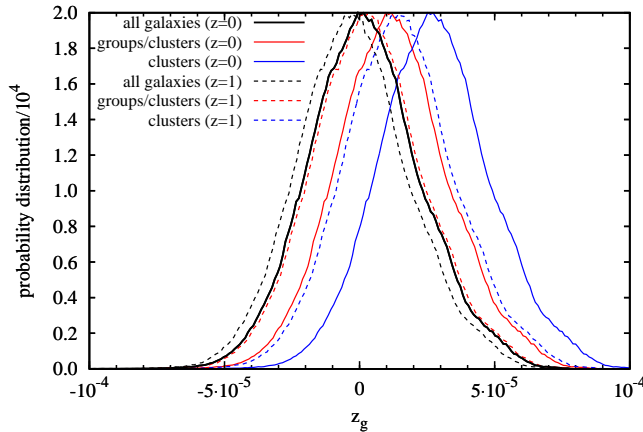


**Figure 2.** Probability distributions of the gravitational redshift at positions of Milky-Way-like galaxies in a large-scale cosmological simulation at cosmological redshift  $z = 0$ . The gravitational redshift is measured from light emitted from all galaxies formed in the simulation (black), galaxies in groups or clusters with a minimum host halo mass of  $10^{13}h^{-1}M_{\odot}$  (red) or  $10^{14}h^{-1}M_{\odot}$  (blue). The widths of the distributions represent a typical scatter in the gravitational potential due to locations of observers in the cosmic web, whereas gradual shifts of the distributions show effect of selecting galaxies in denser environments (solid red and blue lines) or at higher redshift  $z = 1$  (dashed lines). Positive (negative) values correspond to the actual redshift (blueshift) of observed spectra.

As a consequence of a flux limitation, most surveys tend to target more luminous galaxies which in turn populate overdense regions of the Universe. Similarly, supernovae surveys may produce more supernova discoveries in denser fields on the sky. This kind of selection can be quite easily incorporated in our calculation by picking galaxies hosted by more massive haloes. The red and blue lines in Fig. 2 show the distributions of the gravitational redshift given by the gravitational potential of galaxies residing in haloes with masses larger than  $10^{13}h^{-1}M_{\odot}$  and  $10^{14}h^{-1}M_{\odot}$ , respectively (with the same set of observers defined by the Milky-Way-like galaxies). The two adopted minimum halo masses correspond to environments defined by selecting groups or clusters of galaxies. It is clearly visible from the plot that selecting galaxies in denser environments increases the probability of redshift against blueshift, i.e. a positive value of the gravitational redshift is more probable than negative.

## 2.2 Time dependence of the gravitational redshift

The above calculations are based on a  $z = 0$  snapshot, therefore they do not account for the time evolution of cosmic structures. A simple way to show this effect is to select galaxies from a higher-redshift snapshot. Here we repeat our calculations for redshift  $z = 1$  which is nearly an upper limit for the currently observed supernovae (there are far fewer at  $z > 1$ ). We consider the same set of observers as before, i.e. observers located in the Milky-Way-like galaxies at  $z = 0$ , and analogous criteria for galaxy selection: all galaxies at  $z = 1$  and two subsets comprising galaxies in haloes with a minimum mass of  $10^{13}h^{-1}M_{\odot}$  and  $10^{14}h^{-1}M_{\odot}$ . The dashed lines in Fig. 2 show the resulting distributions of the gravitational redshift.

Comparing the gravitational redshift distributions from  $z = 1$  and  $z = 0$  galaxies, we see effect of a gradual decrease of the mean gravitational potential with increasing cosmological redshift: peaks of the  $z = 1$  distributions are blueshifted with respect to their counterparts at



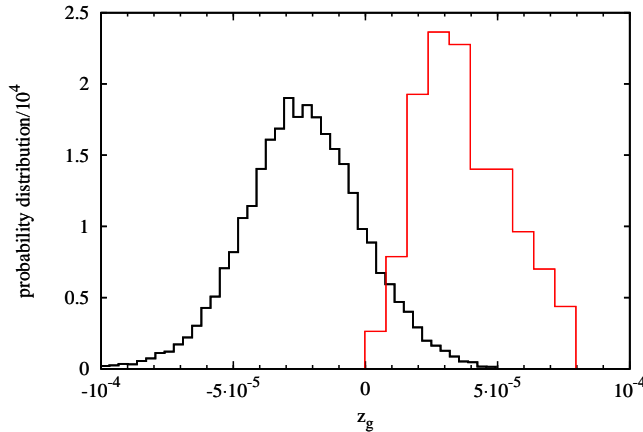


**Figure 3.** Probability distribution of the gravitational redshift measured inside cosmic voids (black) or galaxy clusters (red) at redshift  $z = 0$ . Observers in underdense environments tend to measure a negative signal (gravitational blueshift), whereas those in galaxy clusters always observe gravitational redshift.

$z = 0$ . This is a very intuitive effect and it is related to the fact that the matter distribution is more homogenous at higher redshifts. Time-dependance of the mean potential is a net effect combining growth of large-scale structures and dark matter haloes. The growth of haloes manifests itself as an offset between  $z = 0$  and  $z = 1$  distributions which increases with the minimum halo mass used for galaxy selection. This dependence on the minimum halo mass results from a time lag between formation times of haloes with different masses [37].

Bearing in mind that the scatter represented by the distributions in Fig. 2 is predominantly determined by the distribution of observers in the cosmic web at  $z = 0$ , it is not surprising that all gravitational redshift distributions have the same width. The offsets of the distributions due to redshift evolution are much smaller than their width. This means that in most practical applications the redshift evolution of the gravitational effect will be small. Moreover, it is reassuring that the bias due to gravitational redshifts will be smaller when observing galaxies at higher- $z$  than at low- $z$  because structures were less evolved than they are now — and thus density contrasts were not as significant.

### 2.3 Observers in extreme environments

The distributions of the gravitational redshifts shown in Fig. 2 rely primarily on the assumed ensemble of observers. Although our choice of Milky-Way-like galaxies is fairly general, it seems to be instructive to explore other possibilities. In order to show a maximized effect of this assumption, we consider two extreme cases: observers located in galaxy clusters or in cosmic voids. Galaxy clusters are identified as dark matter haloes with a minimum mass of  $10^{14}h^{-1}M_{\odot}$ . Voids are found using ZOBOV void finder [38] and observers are placed at locations of the minimum density smoothed at a scale of  $10h^{-1}\text{Mpc}$ . We only consider the largest voids with a minimum effective radius of  $100h^{-1}\text{Mpc}$ . Fig. 3 shows the resulting distributions of the gravitational redshift as measured from observations of all galaxies at  $z = 0$ . As expected, observers in voids tend to measure a negative signal (gravitational blueshift), whereas those in galaxy clusters always observe gravitational redshift. Needless to



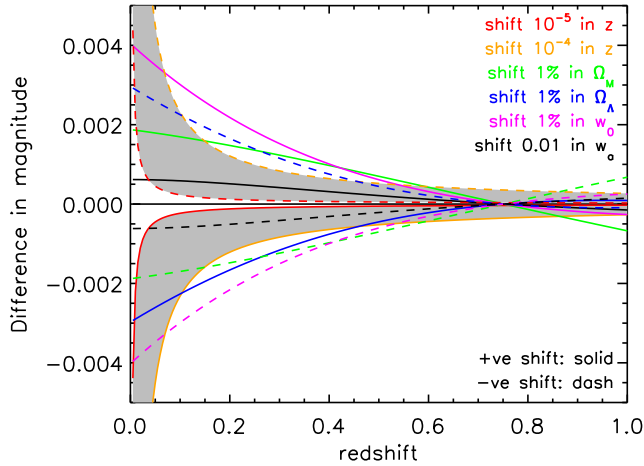


**Figure 4.** How a gravitational redshift changes the magnitude-redshift diagram, in comparison to how it is changed by shifts in cosmological parameters. The horizontal axis is the observed redshift. The shaded regions show how the magnitude-redshift relation is altered with respect to a fiducial  $\Lambda$ CDM model, caused by the presence of the gravitational redshift ranging from  $10^{-5}$  to  $10^{-4}$  (solid lines for a positive redshift, dashed lines for a negative redshift). They are compared to analogous changes obtained by small perturbations of cosmological parameters in the fiducial model. Changes due to a gravitational redshift of  $10^{-5}$ – $10^{-4}$  can be partially mimicked by  $\sim 1\%$  perturbations in some cosmological parameters. Supernova surveys with limited redshift range are particularly sensitive, because marginalising over absolute magnitude effectively allows an arbitrary vertical scaling.

say, both distributions sample respectively the lower and upper tails of the  $z = 0$  distributions shown in Fig. 2.

### 3 Effect of gravitational redshift in analysis of SN Ia data

Cosmological inference with SN data relies primarily on fitting the slope of the magnitude-redshift relation (or, equivalently, the distance modulus-redshift relation) and its dependance on cosmological redshift. The absolute normalization of this relation is degenerate with the Hubble constant and it is commonly treated as a nuisance parameter. Dependence of the apparent magnitude on cosmological redshift is strong enough, especially at small redshifts, to make the magnitude-redshift relation sensitive to quite small perturbations in redshift space. Even for perturbations as small as those given by the expected gravitational redshift due to large-scale structures, deviations in the distance modulus are large enough to have an impact on the measurement of cosmological parameters using SN data. This property is illustrated in Fig. 4 which shows deviations of distance moduli (or apparent magnitude) from a fiducial  $\Lambda$ CDM model due to the presence of the local gravitational redshift. These deviations are compared to analogous changes in the magnitude caused by introducing small perturbations in cosmological parameters with respect to their fiducial values. It is apparent from this figure how perturbing the data by a gravitational redshift induced by large-scale inhomogeneities can partially mimic small changes in cosmological parameters. This means that the presence of the gravitational redshift is expected to affect determination of cosmological parameters with SN data.

Following the main idea illustrated in Fig. 4, here we quantify the impact of the gravitational redshift on cosmological parameters determined from SN data. The effect is measured by fitting cosmological parameters to a mock SN data set generated for a fiducial cosmological model and perturbed by the gravitational redshift. As a fiducial model we assume a flat  $\Lambda$ CDM model with  $\Omega_m = 0.3$  and  $\Omega_\Lambda = 0.7$ . This model is used to calculate distances to and thus distance moduli of SNe. The mock data set comprises redshifts and errors in the apparent magnitude of all 557 SNe Ia from the Union2 compilation [39]. We assume that these redshifts are exact cosmological redshifts which are then perturbed by applying a systematic shift due to the local gravitational redshift. As shown in the previous section (and Fig. 2), the time evolution of the gravitational redshift since redshift  $z = 1$  is small compared to a scatter due to the distribution of observers in the cosmic web. Therefore, for the purposes of this paper it is safe to assume that the perturbation due to gravitational redshift is independent of cosmological redshift.

We fit a cosmological model to the mock SN data by minimizing the posterior probability marginalized over the normalization of the distance modulus-redshift relation. In this approach, the normalization is a nuisance parameter combining the absolute magnitude and the Hubble constant and no prior knowledge of its value is assumed in the analysis. As shown by [40], the logarithm of the posterior probability marginalized over the normalization parameter is given by

$$\chi^2(\theta) \propto \sum \frac{[\mu_i - \mu(\theta, z_i)]^2}{\sigma_i^2} - \frac{\left(\sum \frac{\mu_i - \mu(\theta, z_i)}{\sigma_i^2}\right)^2}{\sum 1/\sigma_i^2}, \quad (3.1)$$

where  $\theta$  is a vector of cosmological parameters,  $z_i$  are cosmological redshifts and  $\sigma_i$  are the errors of the apparent magnitudes. The variable  $\mu$  is a normalization-free distance modulus defined as

$$\mu = 5 \log_{10}(d_L), \quad (3.2)$$

where  $d_L$  is a Hubble-free luminosity distance given by

$$d_L(z) = \begin{cases} (1+z) \sin(I\sqrt{-\Omega_k})/\sqrt{-\Omega_k}, & \Omega_k < 0 \\ (1+z)I, & \Omega_k = 0 \\ (1+z) \sinh(I\sqrt{\Omega_k})/\sqrt{\Omega_k}, & \Omega_k > 0, \end{cases} \quad (3.3)$$

with

$$\Omega_k = 1 - \Omega_m - \Omega_\Lambda, \quad (3.4)$$

$$I = \int_0^z \frac{dz'}{H(z')/H_0}, \quad (3.5)$$

$$H(z)/H_0 = \sqrt{\Omega_m(1+z)^3 + \Omega_\Lambda + \Omega_k(1+z)^2}. \quad (3.6)$$

The  $\mu$  variable is directly related to the apparent magnitude  $m$  through the following relation

$$m = \mu + 25 + M + 5 \log_{10}(c/H_0), \quad (3.7)$$

where  $M$  is the absolute magnitude.

Fig. 5 shows results of fitting  $\Omega_m$  and  $\Omega_\Lambda$  to the mock SN data, as a function of the assumed gravitational redshift. The left panel shows the relative deviations of the best fit parameters

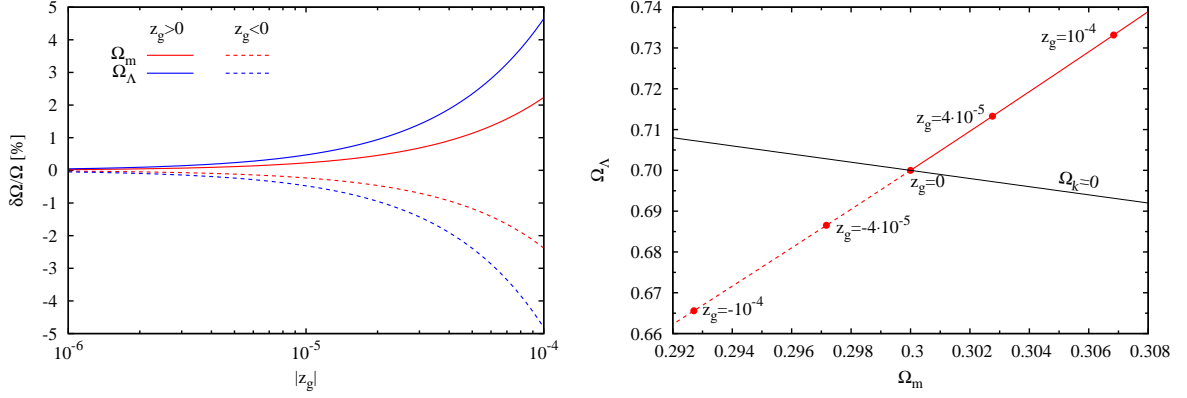


**Figure 5.** Results of fitting a non-flat  $\Lambda$ CDM cosmological model to the mock SN data generated for a fiducial flat  $\Lambda$ CDM model with  $\Omega_m = 0.3$  and  $\Omega_\Lambda = 0.7$  and perturbed by the gravitational redshift due to the local gravitational potential. *Left panel:* The relative deviation of the best fit parameters from the fiducial values as a function of the absolute magnitude of the gravitational redshift. The red and blue curves correspond to a positive and negative gravitational redshift. *Right panel:* Migration of the best fit point on the plane of the density parameters. The black line shows flat  $\Lambda$ CDM models.

from the fiducial values and the right one shows a migration of the best fit point on the plane spanned by the two density parameters. It is clearly readable from this plot that the gravitational redshift has a noticeable effect on measuring cosmological parameters from SN data. A positive gravitational redshift (corresponding to a local underdensity) gives rise to an increase of the best fit density parameter at  $z_g \leq 5 \times 10^{-5}$  by up to 1% for  $\Omega_m$  and up to 3% for  $\Omega_\Lambda$ . This leads effectively to a positive curvature with  $0 < \Omega_k \leq 0.024$ . For negative values of the gravitational redshift, both density parameters are biased low and the relative deviations are approximately symmetric to their counterparts with a positive gravitational redshift. The best fit parameters are distributed along a line which is oriented in a similar way as a degeneracy axis for a cosmological fit based on a non-flat  $\Lambda$ CDM model [see e.g. 39].

Having shown that the gravitational redshift has a noticeable impact on the accuracy of measuring density of dark energy, it is instructive to consider whether constraints on the equation of state should be a matter of similar concern as well. Here we repeat cosmological fits assuming a flat cosmological model with a constant equation of state  $w$ . The Hubble parameter in this case is given by:

$$H(z)/H_0 = \sqrt{\Omega_m(1+z)^3 + \Omega_x(1+z)^{3(1+w)}}, \quad (3.8)$$

where  $\Omega_x$  is the density parameter for dark energy. Fig. 6 shows differences between the best fit  $\Omega_m$  and  $w$ , and the fiducial values, i.e.  $\Omega_m = 0.3$  and  $w = -1$ . Compared to a cosmological fit with a  $\Lambda$ CDM parametrization, the presence of the gravitational redshift leads to opposite biases in  $\Omega_m$  and  $w$ . A positive gravitational redshift increases the value of  $\Omega_m$  and decreases the value of  $w$ . A change of the sign in the gravitational redshift reverses the signs of the biases keeping approximately the same absolute values. In general, effect of the gravitational redshift is stronger than for a  $\Lambda$ CDM fit. Similarly to a fit with a  $\Lambda$ CDM model, the line of best fit models in the parameter space resembles a degeneracy axis for a fit with a flat model and free equation of state  $w$  [see e.g. 39].

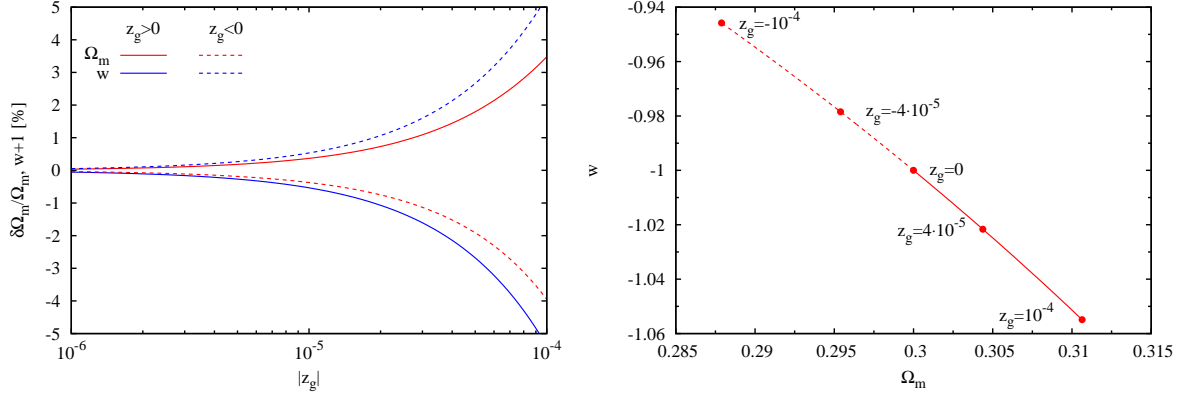


**Figure 6.** Results of fitting a flat cosmological model with a free equation of state for dark energy, to the mock SN data generated for a fiducial flat  $\Lambda$ CDM model with  $\Omega_m = 0.3$  and  $\Omega_\Lambda = 0.7$  and perturbed by the gravitational redshift due to the local gravitational potential. *Left panel:* The relative deviation of the best fit parameters from the fiducial values as a function of the absolute magnitude of the gravitational redshift. The solid and dashed lines correspond to a positive and negative gravitation redshift, respectively. *Right panel:* Migration of the best fit point on the plane of  $\Omega_m$  and  $w$ .

In general, adding more degrees of freedom in cosmological model is expected to amplify deviations from the correct cosmological models. As an ultimate example we consider a cosmological model with a time-dependent equation of state for dark energy. We assume equation of state which is a linear function of the scale factor [41],

$$w(a) = w_0 + w_a(1 - a), \quad (3.9)$$

which yields the following redshift dependence of the Hubble parameter

$$H(z)/H_0 = \sqrt{\Omega_m(1+z)^3 + \Omega_x f(z)}, \quad (3.10)$$

$$f(z) = (1+z)^{3(1+w_0+w_a)} \exp[-3w_a z/(1+z)]$$

As in the previous case, we assume a flat cosmological model. Fig. 7 shows deviations of the best fit parameters obtained from fits assuming a fixed or varying  $\Omega_m$ . When keeping  $\Omega_m$  fixed at its true value, deviations in  $w_a$  are 3 times larger than in  $w_0$  which in turn exhibits nearly the same relative deviations as  $w$  in a cosmological fit with a constant equation of state. A dramatic boost of the deviations is visible when one allows  $\Omega_m$  to vary. In this case, best fit values of  $w_a$  and  $\Omega_m$  for gravitational redshift  $z_g = \pm 5 \times 10^{-5}$  deviate by as much as 40% and  $\pm 3\%$  from their true values. Stronger deviations at  $z_g \geq 7 \times 10^{-5}$  occur when  $w_0 + w_a$  becomes comparable to 0. This part of parameter space violates early dark matter domination and it can be excluded by the CMB and BAO data [39]. Note that if the gravitational redshift effect is important (if we are in a region of the universe experiencing  $z_g \gtrsim 10^{-5}$ ) then an apparent tension between data sets would emerge until this effect was taken into account.

### 3.1 Predictions for systematic errors

There are two possible ways of dealing with the gravitational redshift effect when inferring cosmological parameters from SN data. Assuming prior knowledge of the exact value of the

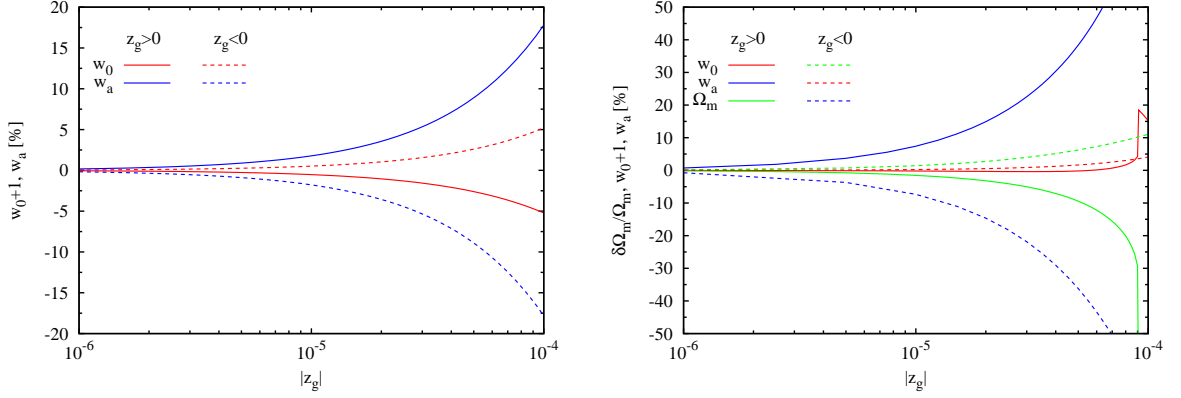


**Figure 7.** Results of fitting a flat cosmological model with  $\Omega_m = 0.3$  but with a free equation of state for dark energy that can vary linearly with scale factor, to the mock SN data generated for a fiducial flat  $\Lambda$ CDM model with  $\Omega_m = 0.3$  and  $\Omega_\Lambda = 0.7$  and perturbed by the gravitational redshift due to the local gravitational potential. The solid and dashed lines show the relative deviation of the best fit parameters from the fiducial values for a positive and negative redshift, respectively. *Left panel:* Results for a model with free parameters of equation of state and fixed density parameters, i.e.  $\Omega_m = 0.3$  and  $\Omega_\Lambda = 0.7$ . *Right panel:* Results for a flat model with free parameters of equation of state. The peculiar behaviour of the  $w_0$  fit at the far right occurs because the best fit  $\Omega_m$  hits zero – which is the edge of the allowable parameter range.

peculiar potential at our own location, one can attempt to correct the observed redshifts for the presence of the gravitational redshift. However, a plausible estimate of the local gravitational potential and thus the gravitational redshift is quite imprecise, because it can only be based on a model of the local density fluctuations and thus it cannot account for a non-negligible contribution from large-scale Fourier modes. Lack of precise observational constraints on the gravitational redshift leads to a second possibility in which the gravitational redshift becomes a source of additional systematic error. In this approach, we accept the fact that the gravitational redshift effect puts limits on the accuracy of cosmological inference using SN data, regardless of amount and quality of the data. Note that this will also affect other distance probes such as baryon acoustic oscillations (BAO). However in the case of BAO the existence of a calibrated standard ruler length (from the CMB) makes the fit more robust because it restricts the overall magnitude shift and thus removes flexibility from the fit.

The systematic errors due to the presence of the gravitational redshift can be calculated by combining results from fitting the mock SN data with the expected distribution of the gravitational redshifts as measured by observers located in the Milky-Way-like galaxies. Since the redshift evolution of the mean potential is much smaller compared to a scatter due to locations of observers in the cosmic web, we only consider the gravitational redshift distribution calculated at cosmological redshift  $z = 0$ . We also conservatively assume that the whole population of galaxies found in the simulation is possibly the least biased representation of a population of the SN Ia host galaxies (see the black curve in Fig. 2).

Fig. 8 shows the distribution of differences between the best fit cosmological parameters and the fiducial values assumed for the SN mock data. Different kinds of lines show results for a non-flat  $\Lambda$ CDM model ( $\Omega_m$  and  $\Omega_\Lambda$ ), a flat  $w$ CDM model with a free equation of state for dark energy ( $\Omega_m$  and  $w$ ), and a flat  $w_a$ CDM model with equation of state linearly dependent

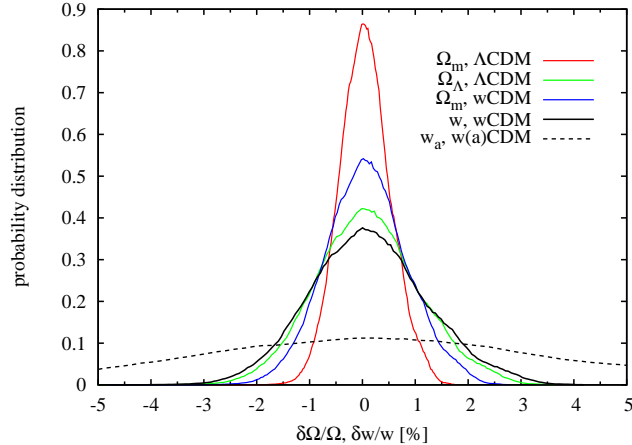


**Figure 8.** Systematic errors in a measurement of cosmological parameters using SN data, due to the presence of an unconstrained gravitational redshift. The curves show the distributions of differences between the best fit cosmological parameters and their fiducial values assumed for the mock SN data. The distributions reflect positions of the Milky-Way-like galaxies in the cosmic web. Cosmological parameters are obtained from two-parameter fits in a non-flat  $\Lambda$ CDM cosmological model with free  $\Omega_m$  and  $\Omega_\Lambda$ , a flat  $w$ CDM model with free  $\Omega_m$  and equation of state  $w$ , or a flat  $w(a)$ CDM model with free  $w_0$  and  $w_a$ .

on the scale factor ( $w_0$  and  $w_a$ ). The standard deviations of the distributions shall be interpreted as systematic errors of the measurement due to the presence of an unconstrained gravitational redshift related to the local gravitational potential. Relative systematic errors amount to 1% and 0.5% for  $\Omega_\Lambda$  and  $\Omega_m$  when fitting a non-flat  $\Lambda$ CDM cosmological model. The corresponding error in  $\Omega_k$  is 0.01. When fitting a flat cosmological model with a free equation of state for dark energy, the expected systematic errors are 0.8% for  $\Omega_m$  and 1.1% for  $w$ . Finally, fitting a flat model with a redshift-dependent equation of state yields systematic error of 3.7% in  $w_a$ . This uncertainty is boosted by a factor of 4 when allowing  $\Omega_m$  to vary.

## 4 Discussion and conclusions

The gravitational redshift due to our own location in the large scale gravitational potential field becomes relevant when using SN data for determination of cosmological parameters to 1% precision. The effect of the gravitational redshift on the best fit models is particularly amplified in extensions of a standard  $\Lambda$ CDM cosmological model such as models invoking dark energy with a redshift-dependent equation of state. These models are of particular attention from the point of view of future dark energy surveys whose goal is to discriminate between a cosmological constant and other forms of dark energy. Our findings imply that neglecting gravitational redshift in a cosmological analysis of SN data leads to an additional systematic uncertainty of 4% in  $w_a$  assuming an unbiased prior on  $\Omega_m$ , and 16% when allowing  $\Omega_m$  to vary.

A cosmological fit with SN data can in principle be corrected for the gravitational redshift effect. This correction would require precise measurement of the gravitational redshift at our location. However, current constraints on the matter distribution in the local universe are not accurate enough, so the only means to account for the gravitational redshift is to consider an

additional systematic error caused by lack of prior knowledge of this redshift. Calculations of these systematic errors presented in this work are based on a matter distribution given by a standard  $\Lambda$ CDM model. This kind of analysis is circular in the sense that results are correct if  $\Lambda$ CDM model is valid. It is a minimum approach in which we show that the presence of the gravitational redshift permitted by a standard cosmological model can mimic certain modifications of the model itself. However, one should bear in mind that other matter distributions for other cosmological models are expected to result in different (and potentially larger) estimates of the systematic errors.

The presence of a gravitational redshift in SN data alters cosmological fits through an alteration in the distance modulus vs redshift relation (see Fig. 4). This issue is worse for supernovae than BAO because for supernovae the combination of absolute magnitude and Hubble parameter is not accurately known, effectively introducing an arbitrary additive scaling to the distance modulus that we need to marginalise over (in Fig. 4 we arbitrarily normalised the theory curves to  $z = 0.8$ ). The BAO length scale can be calibrated to the CMB (or theory), reducing the flexibility in the fit. When considering BAO without a CMB calibration, one would expect a similar effect, except in the opposite direction because  $D_A$  is  $D$  divided by  $(1 + z)$  while  $D_L$  is  $D$  multiplied by  $(1 + z)$ , where  $D$  is the comoving distance,  $D_L$  is the luminosity distance and  $D_A$  is the angular diameter distance. While the relation  $D_L = D_A(1 + z)$  must hold in any metric theory of gravity, in practise this distance duality can be broken because during the analysis the redshift has been mis-assumed to be entirely cosmological.

To conclude, we have shown that our local gravitational environment does affect our cosmological inferences at a level that is important when we are aiming to achieve percent-level accuracy.

## Acknowledgments

We thank Krzysztof Bolejko, David Parkinson and Risa Wechsler for useful discussions. TMD acknowledges the support of the Australian Research Council through a Future Fellowship, grant FT100100595. RW acknowledges support through the Porat Postdoctoral Fellowship. The Dark Cosmology Centre is funded by the Danish National Research Foundation.

## References

- [1] B. Sinclair, T. M. Davis, and T. Haugbølle, *Residual Hubble-bubble Effects On Supernova Cosmology*, *ApJ* **718** (Aug., 2010) 1445–1455, [[arXiv:1006.0911](#)].
- [2] T. M. Davis, L. Hui, J. A. Frieman, T. Haugbølle, R. Kessler, B. Sinclair, J. Sollerman, B. Bassett, J. Marriner, E. Mörtzell, R. C. Nichol, M. W. Richmond, M. Sako, D. P. Schneider, and M. Smith, *The Effect of Peculiar Velocities on Supernova Cosmology*, *ApJ* **741** (Nov., 2011) 67, [[arXiv:1012.2912](#)].
- [3] V. Marra, M. Pääkkönen, and W. Valkenburg, *Uncertainty on  $w$  from large-scale structure*, *MNRAS* **431** (May, 2013) 1891–1902, [[arXiv:1203.2180](#)].
- [4] W. Valkenburg, M. Kunz, and V. Marra, *Intrinsic uncertainty on the nature of dark energy*, *Physics of the Dark Universe* **2** (Dec., 2013) 219–223, [[arXiv:1302.6588](#)].



- [5] L. Amendola, K. Kainulainen, V. Marra, and M. Quartin, *Large-Scale Inhomogeneities May Improve the Cosmic Concordance of Supernovae*, *Physical Review Letters* **105** (Sept., 2010) 121302, [[arXiv:1002.1232](#)].
- [6] D. Sarkar, A. Amblard, D. E. Holz, and A. Cooray, *Lensing and Supernovae: Quantifying the Bias on the Dark Energy Equation of State*, *ApJ* **678** (May, 2008) 1–5, [[arXiv:0710.4143](#)].
- [7] M. Smith, D. J. Bacon, R. C. Nichol, H. Campbell, C. Clarkson, R. Maartens, C. B. D’Andrea, B. A. Bassett, D. Cinabro, D. A. Finley, J. A. Frieman, L. Galbany, P. M. Garnavich, M. D. Olmstead, D. P. Schneider, C. Shapiro, and J. Sollerman, *The Effect of Weak Lensing on Distance Estimates from Supernovae*, *ApJ* **780** (Jan., 2014) 24, [[arXiv:1307.2566](#)].
- [8] I. Zehavi, A. G. Riess, R. P. Kirshner, and A. Dekel, *A Local Hubble Bubble from Type Ia Supernovae?*, *ApJ* **503** (Aug., 1998) 483–491, [[astro-ph/9802252](#)].
- [9] S. Jha, A. G. Riess, and R. P. Kirshner, *Improved Distances to Type Ia Supernovae with Multicolor Light-Curve Shapes: MLCS2k2*, *ApJ* **659** (Apr., 2007) 122–148, [[astro-ph/0612666](#)].
- [10] A. Conley, R. G. Carlberg, J. Guy, D. A. Howell, S. Jha, A. G. Riess, and M. Sullivan, *Is There Evidence for a Hubble Bubble? The Nature of Type Ia Supernova Colors and Dust in External Galaxies*, *ApJ* **664** (July, 2007) L13–L16, [[arXiv:0705.0367](#)].
- [11] J.-S. Huang, L. L. Cowie, J. P. Gardner, E. M. Hu, A. Songaila, Wainscoat, and R. J., *The Hawaii K-Band Galaxy Survey. II. Bright K-Band Imaging*, *ApJ* **476** (Feb., 1997) 12–21, [[astro-ph/9610084](#)].
- [12] W. J. Frith, G. S. Busswell, R. Fong, N. Metcalfe, and T. Shanks, *The local hole in the galaxy distribution: evidence from 2MASS*, *MNRAS* **345** (Nov., 2003) 1049–1056, [[astro-ph/0302331](#)].
- [13] G. S. Busswell, T. Shanks, W. J. Frith, P. J. Outram, N. Metcalfe, and R. Fong, *The local hole in the galaxy distribution: new optical evidence*, *MNRAS* **354** (Nov., 2004) 991–1004, [[astro-ph/0302330](#)].
- [14] I. K. Baldry, K. Glazebrook, and S. P. Driver, *On the galaxy stellar mass function, the mass-metallicity relation and the implied baryonic mass function*, *MNRAS* **388** (Aug., 2008) 945–959, [[arXiv:0804.2892](#)].
- [15] J. R. Whitbourn and T. Shanks, *The local hole revealed by galaxy counts and redshifts*, *MNRAS* **437** (Jan., 2014) 2146–2162, [[arXiv:1307.4405](#)].
- [16] R. C. Keenan, A. J. Barger, and L. L. Cowie, *Evidence for a  $\sim 300$  Megaparsec Scale Under-density in the Local Galaxy Distribution*, *ApJ* **775** (Sept., 2013) 62, [[arXiv:1304.2884](#)].
- [17] H. Böhringer, G. Chon, M. Bristow, and C. A. Collins, *The extended ROSAT-ESO Flux-Limited X-ray Galaxy Cluster Survey (REFLEX II). V. Exploring a local underdensity in the southern sky*, *A&A* **574** (Feb., 2015) A26, [[arXiv:1410.2172](#)].
- [18] R. Wojtak, S. H. Hansen, and J. Hjorth, *Gravitational redshift of galaxies in clusters as predicted by general relativity*, *Nature* **477** (Sept., 2011) 567–569, [[arXiv:1109.6571](#)].
- [19] M. J. d. L. Domínguez Romero, D. García Lambas, and H. Muriel, *An improved method for the identification of galaxy systems: measuring the gravitational redshift by dark matter haloes*, *MNRAS* **427** (Nov., 2012) L6–L10.
- [20] I. Sadeh, L. L. Feng, and O. Lahav, *Gravitational Redshift of Galaxies in Clusters from the Sloan Digital Sky Survey and the Baryon Oscillation Spectroscopic Survey*, *Physical Review Letters* **114** (Feb., 2015) 071103, [[arXiv:1410.5262](#)].
- [21] P. Jimeno, T. Broadhurst, J. Coupon, K. Umetsu, and R. Lazkoz, *Comparing gravitational redshifts of SDSS galaxy clusters with the magnified redshift enhancement of background BOSS galaxies*, *MNRAS* **448** (Apr., 2015) 1999–2012, [[arXiv:1410.6050](#)].

- [22] A. Cappi, *Gravitational redshift in galaxy clusters.*, *A&A* **301** (Sept., 1995) 6.
- [23] Y.-R. Kim and R. A. C. Croft, *Gravitational Redshifts in Simulated Galaxy Clusters*, *ApJ* **607** (May, 2004) 164–174, [[astro-ph/0402047](#)].
- [24] H. Zhao, J. A. Peacock, and B. Li, *Testing gravity theories via transverse Doppler and gravitational redshifts in galaxy clusters*, *Phys. Rev. D* **88** (Aug., 2013) 043013, [[arXiv:1206.5032](#)].
- [25] N. Kaiser, *Measuring gravitational redshifts in galaxy clusters*, *MNRAS* **435** (Oct., 2013) 1278–1286, [[arXiv:1303.3663](#)].
- [26] R. A. C. Croft, *Gravitational redshifts from large-scale structure*, *MNRAS* **434** (Oct., 2013) 3008–3017, [[arXiv:1304.4124](#)].
- [27] P. J. E. Peebles, *The large-scale structure of the universe*. Princeton University Press, 1980.
- [28] J. A. Muñoz and A. Loeb, *The density contrast of the Shapley supercluster*, *MNRAS* **391** (Dec., 2008) 1341–1349, [[arXiv:0805.0596](#)].
- [29] J. A. Peacock, *Cosmological Physics*. Cambridge University Press, Jan., 1999.
- [30] K. Riebe, A. M. Partl, H. Enke, J. Forero-Romero, S. Gottlöber, A. Klypin, G. Lemson, F. Prada, J. R. Primack, M. Steinmetz, and V. Turchaninov, *The MultiDark Database: Release of the Bolshoi and MultiDark cosmological simulations*, *Astronomische Nachrichten* **334** (Aug., 2013) 691–708.
- [31] E. Komatsu, J. Dunkley, M. R. Nolte, C. L. Bennett, B. Gold, G. Hinshaw, N. Jarosik, D. Larson, M. Limon, L. Page, D. N. Spergel, M. Halpern, R. S. Hill, A. Kogut, S. S. Meyer, G. S. Tucker, J. L. Weiland, E. Wollack, and E. L. Wright, *Five-Year Wilkinson Microwave Anisotropy Probe Observations: Cosmological Interpretation*, *ApJS* **180** (Feb., 2009) 330–376, [[arXiv:0803.0547](#)].
- [32] V. Springel, *The cosmological simulation code GADGET-2*, *MNRAS* **364** (Dec., 2005) 1105–1134, [[astro-ph/0505010](#)].
- [33] A. Klypin and J. Holtzman, *Particle-Mesh code for cosmological simulations*, *ArXiv Astrophysics e-prints* (Dec., 1997) [[astro-ph/9712217](#)].
- [34] Z. Zheng, A. A. Berlind, D. H. Weinberg, A. J. Benson, C. M. Baugh, S. Cole, R. Davé, C. S. Frenk, N. Katz, and C. G. Lacey, *Theoretical Models of the Halo Occupation Distribution: Separating Central and Satellite Galaxies*, *ApJ* **633** (Nov., 2005) 791–809, [[astro-ph/0408564](#)].
- [35] R. Wojtak, A. Knebe, W. A. Watson, I. T. Iliev, S. Heß, D. Rapetti, G. Yepes, and S. Gottlöber, *Cosmic variance of the local Hubble flow in large-scale cosmological simulations*, *MNRAS* **438** (Feb., 2014) 1805–1812, [[arXiv:1312.0276](#)].
- [36] Y.-S. Li and S. D. M. White, *Masses for the Local Group and the Milky Way*, *MNRAS* **384** (Mar., 2008) 1459–1468, [[arXiv:0710.3740](#)].
- [37] R. H. Wechsler, J. S. Bullock, J. R. Primack, A. V. Kravtsov, and A. Dekel, *Concentrations of Dark Halos from Their Assembly Histories*, *ApJ* **568** (Mar., 2002) 52–70, [[astro-ph/0108151](#)].
- [38] M. C. Neyrinck, *ZOBOV: a parameter-free void-finding algorithm*, *MNRAS* **386** (June, 2008) 2101–2109, [[arXiv:0712.3049](#)].
- [39] R. Amanullah, C. Lidman, D. Rubin, G. Aldering, P. Astier, K. Barbary, M. S. Burns, A. Conley, K. S. Dawson, S. E. Deustua, M. Doi, S. Fabbro, L. Faccioli, H. K. Fakhouri, G. Folatelli, A. S. Fruchter, H. Furusawa, G. Garavini, G. Goldhaber, A. Goobar, D. E. Groom, I. Hook, D. A. Howell, N. Kashikawa, A. G. Kim, R. A. Knop, M. Kowalski, E. Linder, J. Meyers, T. Morokuma, S. Nobili, J. Nordin, P. E. Nugent, L. Östman, R. Pain, N. Panagia, S. Perlmutter, J. Raux, P. Ruiz-Lapuente, A. L. Spadafora, M. Strovink, N. Suzuki, L. Wang, W. M. Wood-Vasey, N. Yasuda, and T. Supernova Cosmology Project, *Spectra and Hubble*

*Space Telescope Light Curves of Six Type Ia Supernovae at  $0.511 < z < 1.12$  and the Union2 Compilation*, *ApJ* **716** (June, 2010) 712–738, [[arXiv:1004.1711](#)].

- [40] M. Goliath, R. Amanullah, P. Astier, A. Goobar, and R. Pain, *Supernovae and the nature of the dark energy*, *A&A* **380** (Dec., 2001) 6–18, [[astro-ph/0104009](#)].
- [41] E. V. Linder, *Exploring the Expansion History of the Universe*, *Physical Review Letters* **90** (Mar., 2003) 091301, [[astro-ph/0208512](#)].